Research Article

Afif Batal*, Aleksandra Michalek, Antonio Garcia-Giron, Vahid Nasrollahi, Pavel Penchev, Rachel Sammons and Stefan Dimov

Effects of laser processing conditions on wettability and proliferation of Saos-2 cells on CoCrMo alloy surfaces

https://doi.org/10.1515/aot-2019-0051
Received September 2, 2019; accepted October 19, 2019; previously published online November 14, 2019

Abstract: Any processing disturbances in laser surface texturing (LST) could compromise the resulting surface topography and their desired functional response. Disturbances such as focal plane offsets and beam incident angle variations are always present in LST processing of 3D parts and can affect the surface morphology. In this research the effects of these laser processing disturbances in producing laser induced surface structures (LIPSS) on CoCrMo alloy substrates were investigated. In particular, these two disturbances were considered as laser processing variables to determine their effects on functional responses of LIPSS treated surfaces, i.e. surface wettability and the proliferation of Saos-2 osteoblast-like cells were evaluated. It was found that the changes of laser processing conditions led to a decrease in surface wettability and Saos-2 cells proliferation. In addition, a correlation between surface wettability and cell proliferation on LIPSS treated surface was identified and conclusions made about the effects of investigated process disturbances on the functional response of LIPSS treated CoCrMo substrates.

Keywords: cobalt chrome molybdenum; laser induced periodic surface structures; laser surface texturing; osseointegration; surface functionalization.

***Corresponding author: Afif Batal,** Department of Mechanical Engineering, University of Birmingham, Edgbaston, Birmingham B15 2TT, UK, e-mail: bxa361@student.bham.ac.uk
Aleksandra Michalek, Antonio Garcia-Giron, Vahid Nasrollahi, Pavel Penchev and Stefan Dimov: Department of Mechanical Engineering, University of Birmingham, Edgbaston, Birmingham B15 2TT, UK. https://orcid.org/0000-0002-5697-8062 (V. Nasrollahi)
Rachel Sammons: School of Dentistry, University of Birmingham, Edgbaston, Birmingham B5 7EG, UK

www.degruyter.com/aot

1 Introduction

The functionalization of surfaces has become an integral part in the design of innovative products with high commercial potential and advanced functionalities. In particular, it allows the embedment of new properties that is foreign to the underlying substrate material, for instance turning a hydrophilic surface into a super hydrophobic one [1], or the enhancement of existing properties such as improving the biological response of Titanium alloys [2].

There are various approaches for functionalizing surfaces such as changing the surface chemistry [3], the material's microstructure on the surface [4] or the surface topography [5] and also some combinations of them. Moreover, there is a diverse range of processes available to achieve such surface functionalities. For example, Gholami et al. investigated the effect of annealing temperature on the pitting corrosion resistance of 2205 duplex stainless steel [6], Zhenyu et al. produced hydrophobic surfaces on PMMA and Ti-6 Al-4V alloy substrates via micro-milling [7], Kumar and Patel improved the cutting performance of Al_2O_3/TiCN composite ceramic tools by producing micro-grooves on their rake surface via WEDM [8], Arisoy et al. produced antibacterial and antifouling surfaces via nanoimprint lithography [9], finally Bang et al. enhanced the biological response of pure titanium via sandblasting and acid etching [10]. Another process that has been attracting a lot of interest recently from both the industry and the research is laser surface texturing (LST). LST offers a number of advantages over competing technologies. In particular, LST can be deployed to process freeform surfaces of most engineering materials selectively, with a relatively higher processing speed and higher accuracy, repeatability and reproducibility [11]. In addition, LST does not involve the use of harmful chemicals and also can represent a relatively low cost option when compared with other unconventional machining processes.

LST was successfully employed by the automotive industry to treat cylinder liners of internal combustion engines and to improve fuel consumption and reduce engine wear [12]. It was also employed as a means of reducing friction and wear between other types of sliding surfaces such as PTFE/Kevlar fabric composites [13], polymers [14], and more [15]. More recently, LST found applications in medical industry, specifically to modify surfaces of orthopedic implants. Shah et al. studied the effect of Nd: YAG laser modification of pure titanium implants on osseointegration and biomechanical anchorage. The modified implants exhibited 153% higher removal torque values in rabbit tibiae when compared to their untreated counterparts. Furthermore, when their fracture toughness was analyzed, fracture lines appeared within the bone for the laser modified implants whereas for the untreated titanium screws, the implants failed at the bone/implant interface [16]. In another study, Briski et al. found that laser modified PEEK implants enhanced fusion in a sheep model and more abundant mineralized matrix and bony attachments were found on the treated implants than in the control group [17].

Laser induced periodic surface structures (LIPSS) are grating-like patterns that can be generated on almost any material when the laser power level is at or near the damage threshold of the workpiece. LIPSS generation is generally attributed to some form of interference between the incident laser beam and the surface-scattered electromagnetic waves [18]. Low spatial frequency (LSFL) LIPSS form on processed surfaces with a spatial period close to the laser wavelength and it is commonly under 1 μm for near infrared sources. This length scale is particularly interesting when dealing with small living organisms, such as bone cells, and therefore LIPSS have a strong potential in the field of biomaterials modification. For example, LIPSS enhanced matrix mineralization and bone-like nodule formation as compared with polished Ti-6 Al-4V surfaces and thus they could potentially improve human mesenchymal stem cells differentiation into osteoblastic lineage [19]. Furthermore, it was shown that LIPSS with different periodicities greatly improved the proliferation of HEK-293 cell line on polystyrene surfaces; the improvement was more pronounced in the later stages of incubation [20]. In a previous study it was shown that a crossed LIPSS patterns enhanced Saos-2 osteoblast-like cell growth on polished cobalt-chromium-molybdenum (CoCrMo) alloy surfaces without compromising on initial cell adhesion, a characteristic of rougher surfaces [21].

It is evident from results of many empirical studies that LST and LIPSS in particular, has a real potential as technology for modifying implant surfaces and therefore it is essential to investigate and determine the process limitations. This is especially necessary when applying LST on freeform surfaces that are common in most implant designs. In particular, when the LST technology is deployed on complex 3D surfaces, there are substantial changes in the laser processing conditions when compared with the processing of planar surfaces. Therefore, the factors impacting the process performance on 3D surfaces should be considered as disturbances affecting the functional response of treated surfaces. Hence, the effects of such disturbances on added functionalities established in numerous empirical studies on planar surfaces should be investigated in order to establish the limitations of the LST technology when applied on 3D surfaces.

This paper reports investigation into the disturbances present in LST of 3D CoCrMo alloy surfaces and their effects on the functional response of such treated surfaces. In particular, the effects of the focal offset distance (FOD), beam incident angle (BIA) and the initial surface quality on the static water contact angle and Saos-2 osteoblast-like cells proliferation have been studied.

2 Materials and methods

2.1 Material and surface analysis methods

A 13 mm diameter CoCrMo disks were used in this study with the composition of 67.0% Co, 27.0% Cr and 5.0% Mo surgical grade CoCrMo casting alloy. The surface roughness of as-received disks was measured and the arithmetical mean height, S_a, and the root mean square height, S_q, values were both around 45 μm. Some disks were polished down to a surface roughness of S_a 40 nm and S_q 60 nm. The surface roughness was measured using an Alicona focus variation microscope.

All disks were examined using a scanning electron microscopy, Zeiss EVO MA 10, with the following settings: WD = 8.0 mm and EHT = 10.00 kV. In addition, the topography of the laser processed samples was examined employing an atomic force microscopy (AFM), Dimension 3100 system with Bruker NP-10 non-conductive silicon nitride tips.

2.2 Laser surface texturing

The CoCrMo disks were laser processed using an ultrashort near-infrared fiber laser with the following technical specification: 5W average power, 10 μJ maximum pulse energy, 310 fs pulse duration, 500 KHz maximum repetition rate, 1030 nm center wavelength and beam quality M^2 better than 1.2. The beam spot size at the focal plane was 40 μm.

Initially, the LIPSS pattern used in this study was optimized by varying the laser parameters on polished CoCrMo disks, employing the method proposed by Gnilitskyi et al. [22]. In particular, the LIPSS

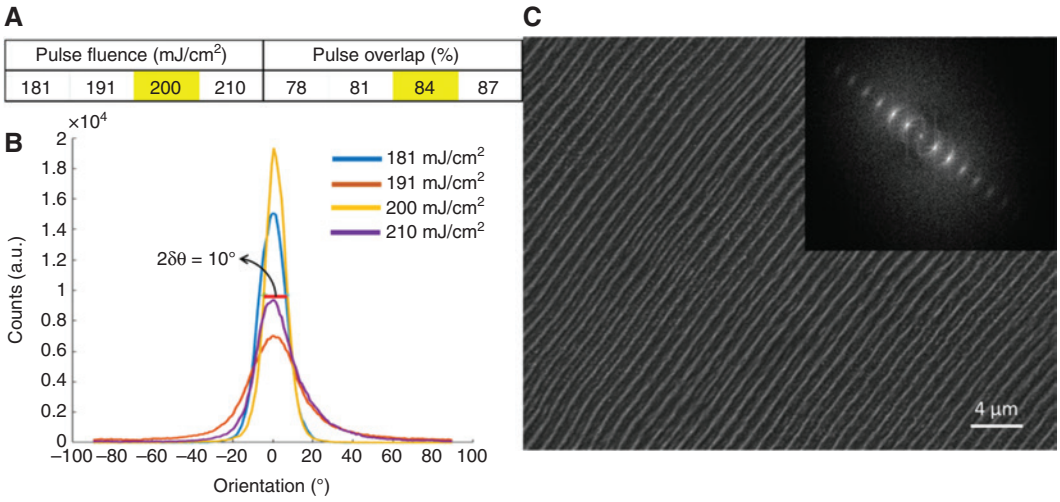

Figure 1: An overview of the conducted process optimization: (A) the processing window considered in a full factorial design of experiments (B) distribution of orientation θ obtained from ImageJ for a fixed overlap of 84% (C) SEM micrograph, and corresponding Fourier transform of a CoCrMo surface processed with the optimized parameters.
Note: Optimized parameters are highlighted in yellow.

optimization process involved an analysis of SEM images and their regularity. Using the open-source software ImageJ with the OrientationJ plug-in and its Orientation Distribution module with Riesz Filters, the distribution angle values were calculated for the different SEM micrographs. All images used in the analysis had the same magnification (6000×) in order to analyze large areas sufficiently. In addition, the spectrum was normalized with the highest value of the distribution shifted to the orientation value of 0°. Then, the value of half width at half maximum was obtained, defined as, the dispersion value of the LIPSS orientation angles (DLOA). The samples with the lowest DLOA (2δθ) were highly-regular and therefore were selected to investigate how process disturbances could affect surface topographies and their respective functionalities in this research. The considered laser parameters, tested in a full factorial design and the optimized textured surface are shown in Figure 1. The pulse overlap was fixed in both x and y directions of scanning.

Then, the optimized laser parameters (Figure 1A) were used on all CoCrMo samples while process disturbances, i.e. FOD, BIA, and material disturbance such as initial surface quality, were introduced to investigate their effects on topography and functional response of LST surfaces. In particular, a set of experiments were conducted with the same laser processing settings while different levels of these three disturbances were applied as shown in Table 1 and Figure 2.

Table 1: The parameters' domain used for LIPSS generation.

Sample	Process-material disturbances		
	Surface quality	FOD (mm)	BIA (°)
1	As-received	0	0
2	As-received	0.2	0
3	As-received	0.4	0
4	As-received	0.6	0
5	As-received	0.8	0
6	As-received	0	10
7	As-received	0	20
8	As-received	0	30
9	Polished	0	0
10	Polished	0.2	0
11	Polished	0.4	0
12	Polished	0.6	0
13	Polished	0.8	0
14	Polished	0	10
15	Polished	0	20
16	Polished	0	30

2.3 Functional analysis of LST surfaces

Prior to functional testing, the samples were rigorously cleaned by two 15 min ultrasonic baths, first, in pure acetone, and then, in 70 vol% ethanol aqueous solution. The disks were rinsed with pure distilled water in between two baths and finally dried with argon gas and stored in sterile petri dishes.

The wetting properties of the LST surfaces were analyzed directly after cleaning. The static contact angle (CA) measurement was performed by employing the sessile drop technique. An Attension Theta optical tensiometer with 6 µl drops of purified Milli-Q water was used to conduct these measurements. The drop volume was selected in such a way that the gravity forces should not be higher than the capillary one, to minimize any additional kinetic energy. In this way the values represented the true solid/liquid interactions.

Saos-2 osteoblast-like cell proliferation on LST CoCrMo disks was analyzed, too. The specimens were then placed in 24-well plates (Thermo Scientific™ Nunc™ Cell-Culture Treated Multidishes) and approximately 1×10^4 Saos-2 osteoblast-like cells were seeded on each sample in McCoy's 5A medium supplemented with 10% fetal bovine serum (FBS), 100 U/ml of penicillin and 100 µg/ml of streptomycin. The well plates were placed in a humidified incubator at 37°C in an atmosphere of 5% CO_2 and the culture medium was changed every 2 days.

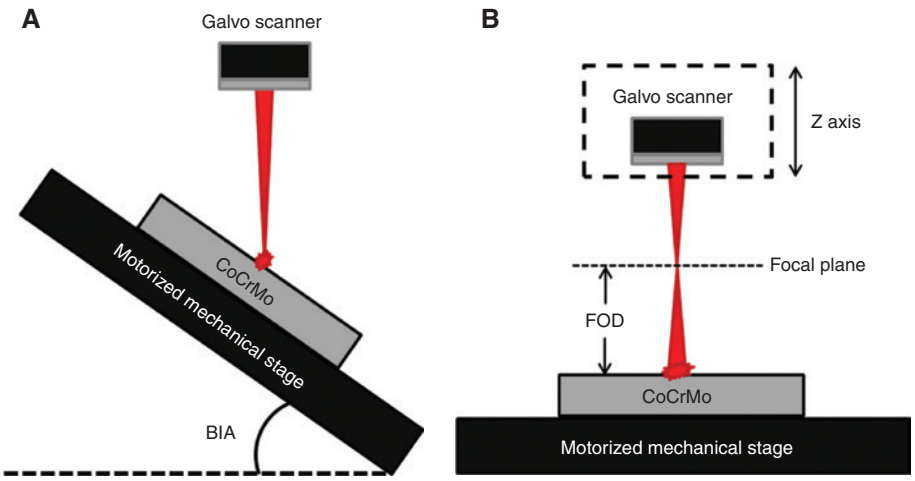

Figure 2: Schematic diagrams of laser processing at different (A) BIA and (B) FOD.

Saos-2 cells metabolic activity was evaluated via a MTT assay [23], reflecting the cells' proliferation on the different CoCrMo specimens. MTT was prepared in phosphate buffered saline (PBS, pH 7.4) with a concentration of 5 mg/ml. 60 µl of the MTT solution was added to each well and the plates were incubated at 37°C in an atmosphere of 5% CO_2 for 4 h at the selected time interval of 4 days after seeding. The medium was then removed and 0.6 ml of DMSO was added to each well to dissolve the formazan. The well plates were placed on a shaking platform for 5 min and then the optical density was measured at 570 nm using a spectrophotometer.

All functional data were expressed as mean and standard deviation, n = 4 for CA and MTT measurements. Statistical analysis was performed using Minitab 17 Statistical Software. A Pearson correlation valuation was conducted to examine the relationship between wettability and cell proliferation on the laser treated disks.

3 Results

3.1 Effects on surface topography

LST was performed on the CoCrMo disks employing the process settings and disturbances that are listed in Table 1. First, the effects of initial surface roughness on resulting surface topography were analyzed. In particular, LST produced different results on the as-received and polished surfaces as depicted in Figure 3. The surface defects on as-received disks (see Figure 3C) led to interruptions in the LIPSS patterns and changes in the ripples' orientation. Moreover, small areas were left untextured, too. At the same time, on polished disks (see Figure 3D), the LIPSS were highly regular, parallel, and uniform while their orientation was perpendicular to the laser polarization vector and covered the surface of the disk completely.

Second, the effects of the beam incident angle on periodicity of produced LIPSS on polished CoCrMo disks were investigated experimentally. In particular, the periodicity of produced LIPSS was assessed by using the Fourier transforms of the SEM images as shown in Figure 4. The periodicity increased with the increase in BIA and was roughly 980, 1140, 1400, and 1770 nm, respectively for incidence angles of 0, 10, 20, and 30°. Furthermore, additional intermediary ripples were formed at 30° their periodicity was 650 nm. No such ripples were observed at processing angles less than 30°.

The theoretical LIPSS periodicity was also calculated. It depends on beam incidence angle and can be expressed as:

$$\Lambda = \lambda / \sqrt{(k_0/k)^2 \pm \sin^2\theta} \quad (1)$$

where λ is the laser wavelength; k_0 is the surface electromagnetic wave propagation constant (function of the material dielectric constants); $k = 2\pi/\lambda$; and θ – the laser beam incidence angle [24]. The p– and p+ variants in Figure 4 are a result of the +/ – sign in Eq. (1). The theoretical periodicity was calculated based on Eq. (1) and then normalized to the measured periodicity at 0° as the values were slightly higher. The empirical and analytical results are compared in Figure 4. The deviation between the theoretical and experimental values was less than 5% and this could be attributed to some processing effects together with some measurement uncertainty and the alloy's real dielectric constants. Overall, there was a strong agreement between the theoretical and experimental trends as depicted in Figure 4. The amplitude of the ripples (the depth of valleys) stayed unchanged when BIA was set at 10 and 20°, however at a 30°, the intermediary ripples had an amplitude of roughly 50 nm.

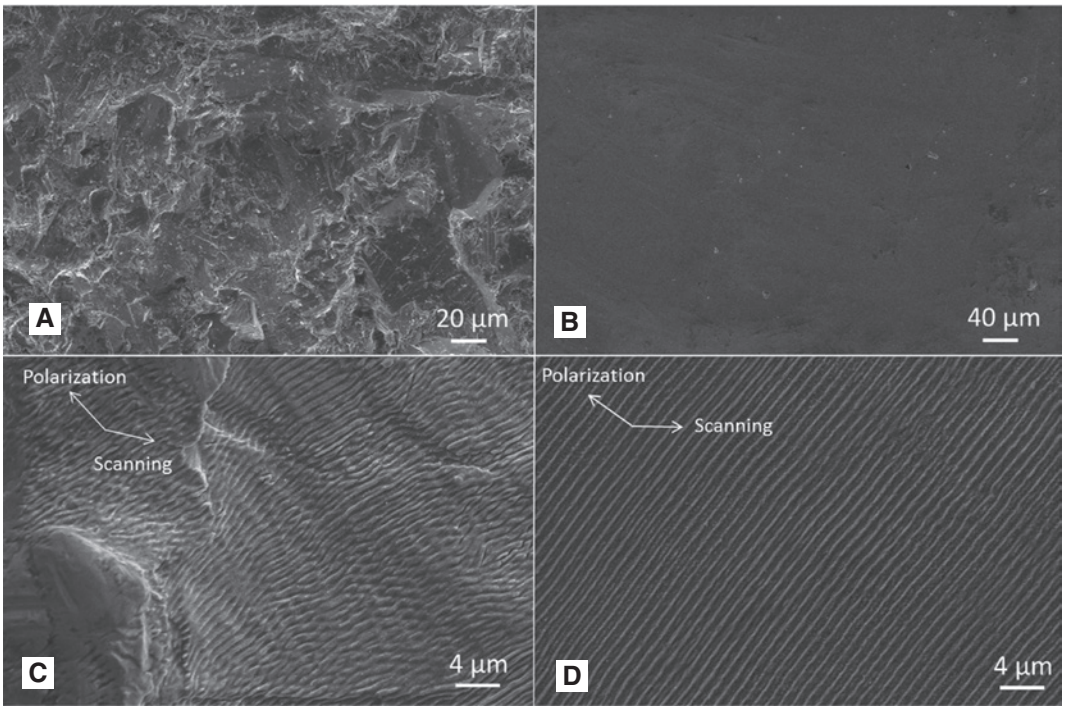

Figure 3: Representative SEM micrographs of (A) as-received and (B) polished (C) laser processed as-received (D) laser processed polished CoCrMo surfaces.
Note: LST was conducted in-control using optimized parameters and without any process disturbances.

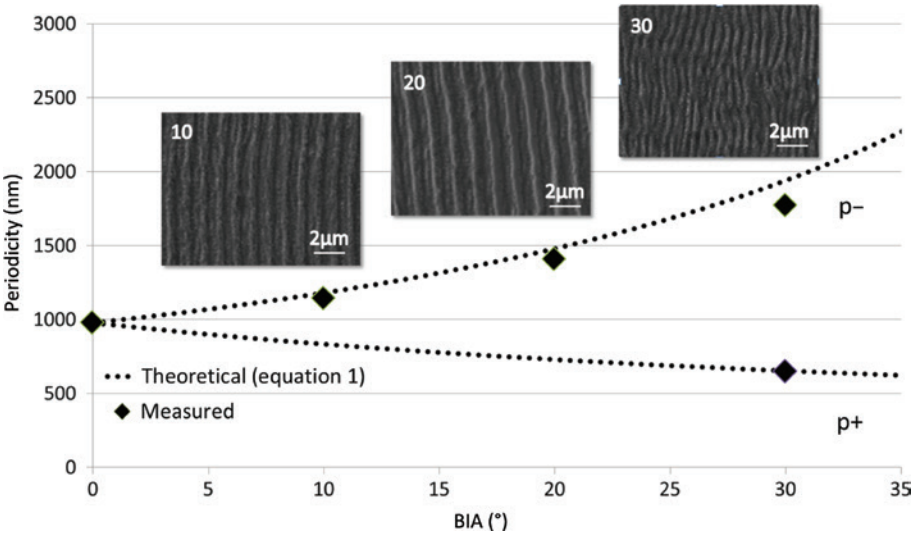

Figure 4: Empirical and analytical LIPSS periodicity at different BIA values on CoCrMo.
Note: The dash line represents the theoretical values while the diamonds the empirical values obtained from the Fourier transforms of the SEM images.

Finally, the effects of the FOD on resulting LIPSS were analyzed. The profiles of the LIPSS were analyzed via AFM and the data is summarized in Figure 5 and Table 2. The average LIPSS amplitude decreased from 115 nm when in focus, down to 35 nm at a defocusing distance of 0.8 mm (see Figure 5). The periodicity of the produced ripples stayed unchanged when FOD was varied.

3.2 Effects on surface functionality

3.2.1 Surface wettability

The LIPSS treatment decreased the wettability both on as-received and polished CoCrMo disks. In particular, the LST process increased the CA values from 57.9° to 63.6° (9.8%)

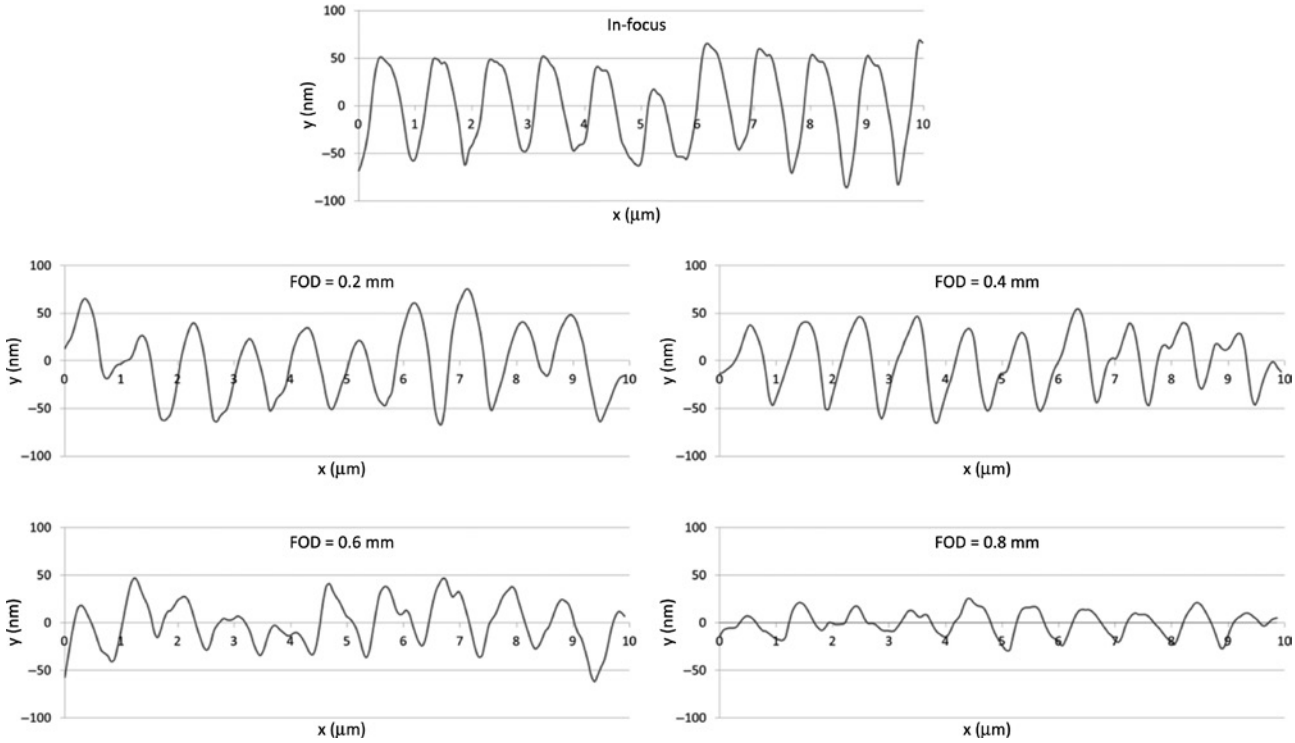

Figure 5: Profile of polished surfaces with LIPSS at different FOD.

Table 2: Summary of the effects of process disturbances on resulting topography.

Sample		Average depth (±10 nm)	Average periodicity (±15 nm)	Representative surface profile
FOD	9	115	980	
	10	105	980	
	11	90	980	
	12	60	980	
	13	35	980	
BIA	14	115	1140	
	15	115	1400	
	16	110 and 50	1770 and 650	

and from 46.0° to 54.7° (19%) on as-received and polished surfaces, respectively, when there was no other processing disturbances present.

The CA values increased further with the increase in BIA as shown in Figure 6. The trend appears to be valid for both as-received and polished surfaces. The CA increased from 63.6° to 76.1° (20%) and from 54.7° to 68.5° (25%) with the increase of the angle of incidence to 30° on as-received and polished disks, respectively.

Finally, the FOD effects on surface wettability were analyzed. The CA values increased initially with the increase of the beam offset to reach a plateau at 0.4 mm offset and then gradually decreased as shown in Figure 7. This tendency was observed both on as-received and polished disks. In particular, 17% and 6% CA increase were observed initially on both disks, respectively, and then the CA values dropped significantly on as-received disks, i.e. from 74.2° to 55.6°, and only a marginal drop from

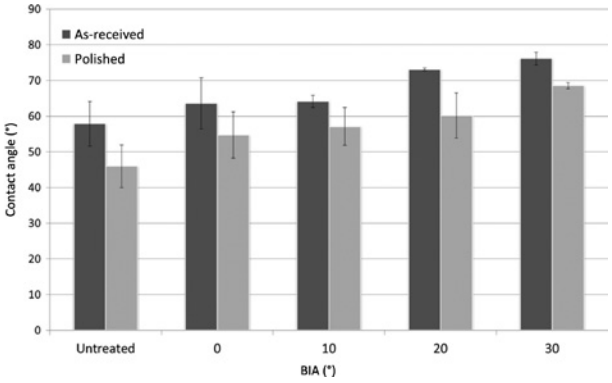

Figure 6: The beam incident angle effects (deg.) on CoCrMo disks' wettability.

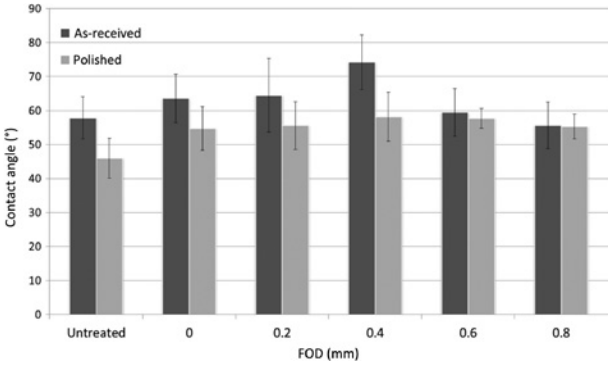

Figure 7: The beam defocusing distance (mm) effects on CoCrMo disks' wettability.

58.1° to 55.3° on polished samples when FOD reached 0.8 mm.

3.2.2 Saos-2 cell proliferation

Overall, LIPSS enhanced the proliferation of the Saos-2 osteoblast-like cells on CoCrMo alloy disks, regardless of their initial surface condition. The highest improvement in cell viability observed was 18.2% and 27.7% for the as-received and polished surfaces, respectively, 4 days after seeding the cells compared with the untreated surfaces.

Generally, higher cell viability was observed on rougher as-received surfaces 4 days after seeding regardless of the laser treatment.

The Saos-2 cell viability decreased with the increase of the laser incidence angle (Figure 8). This is the case for both as-received and polished surfaces. The optical density decreased from 0.155 to 0.111 (27.7%) and from 0.149 to 0.109 (26.8%) for the as-received and polished surfaces with the increase of the incidence angle to 30°, respectively.

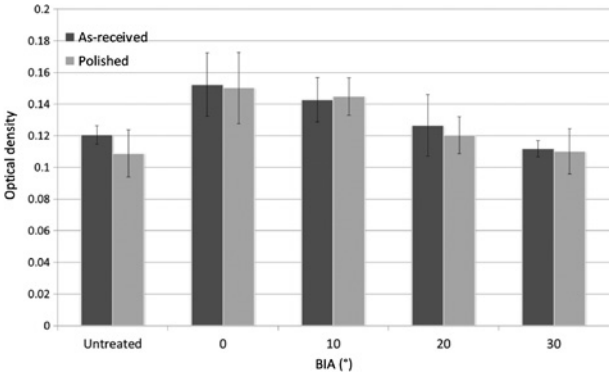

Figure 8: The beam incident angle (deg.) influence on proliferation of Saos-2 cells on textured CoCrMo disks 4 days after seeding.

A loss of the added cell proliferation improvement via LST is apparent when the BIA is increased past 25°, indeed, higher optical density values were obtained on untreated surfaces compared to those that were processed with 30° BIA.

A similar trend in regards to the cell viability was observed initially with the FOD increase and the lowest values were obtained at FOD of 0.4 mm. Then, there was a gradual increase with any further focus offset as shown in Figure 9 and this trend was observed on both as-received and polished surfaces. In particular, the optical density decreased initially from 0.155 to 0.126 (18.5%) and 0.149 to 0.123 (17%) when FOD reached 0.4 mm before it started to increase to 0.141 and 0.137 at 0.8 mm defocusing distance on as-received and polished surfaces, respectively.

Therefore, looking at the CA and proliferation data, there is an inverse correlation between CA and the proliferation of Saos-2 cells on the laser-treated CoCrMo alloy disks, regardless of their initial surface quality. The same trend was observed when cell viability measurements

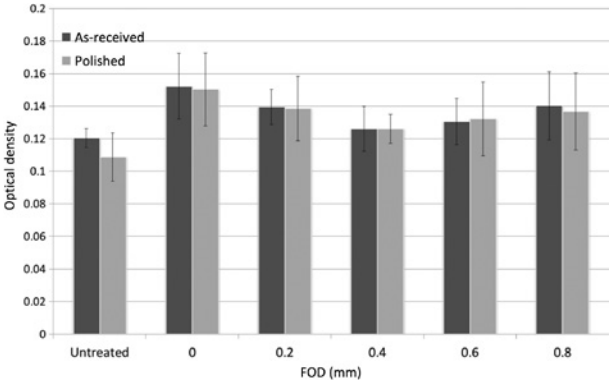

Figure 9: The beam defocusing distance (mm) influence on proliferation of Saos-2 cells on textured CoCrMo disks 4 days after seeding.

Table 3: Pearson correlation results.

Laser processing condition	Pearson correlation coefficient	*p*-Value
As-received/incident angle	−0.974	0.026
As-received/off-focus	−0.411	0.492
Polished/incident angle	−0.973	0.027
Polished/off-focus	−0.896	0.04

were taken 2 days after seeding (data not shown), however the biological improvement was more pronounced after 4 days. The Pearson correlation results for the laser processed samples are shown in Table 3. It is worth noting that the effects of BIA on the functional response of the surface are more pronounced than those of FOD; the statistical significance of the results is greater when the BIA is changed and less when the FOD is changed.

4 Discussion

The conducted empirical study has shown clearly that changes in the LST conditions, i.e. the presence of disturbances common in laser processing of 3D surfaces, alter the functionality of laser-processed surfaces. Therefore, the effects of such process disturbances, i.e. initial surface roughness, FOD, and BIA, should be considered carefully when LST 'recipes' developed and tested on planar substrates are applied on freeform surfaces, for example when processing implants. The ranges within which the desired surface functional response is still within some pre-defined limits in the presence of these process disturbances should be determined. In this way, it will be possible to define/design LST strategies that allow the surface functionality to be maintained within acceptable limits dictated by any specific application.

When the process is in control (no presence of LST disturbances) LST leads to a decrease of the CoCrMo disks' wettability. This indicates that despite the samples remaining relatively hydrophilic (CA < 90°), they exhibited a Cassie-Baxter (CB) state of wetting, where air entrapped in the surface roughness contributed to the decrease in wettability. According to Giacomello et al., the CB state at the nanoscale can be stable in the case of moderate hydrophilic surfaces [25]. The experimental results in this research are in line with Giacomello's analysis, as the introduction of sub-micron surface topography did not increase the wettability of the initially hydrophilic surface. Furthermore the introduction of LIPSS was shown to increase the CA on AISI 316L and Ti–6Al–V surfaces further reaffirming the CB theory [26].

The laser processing treatment improved the biological response of the CoCrMo alloy disks, regardless of their initial surface quality as expected, based on the literature and previous work [19–21].

The effects of each of the three LST disturbances, the initial surface quality, BIA, and FOD on the static water contact angle and Saos-2 osteoblast-like cell proliferation are discussed separately in the following Sections.

4.1 Effects of initial surface quality

The irregularity of the rough surface influenced the formation, morphology, and orientation of the LIPSS on the as-received CoCrMo alloy disks. In particular, defects such as small holes, grains, and scratches disrupted the regular orientation of ripples that are normally perpendicular to the polarization vector. Such defects may result in surface strain which overpowers the laser electric field governing the formation direction of the LST generated sub-micron structures. Similar findings were observed on calcium fluoride and poly-carbonate films [27, 28]. Moreover, morphological differences related to process disturbances such as off-focus processing and BIA variations were observed also on in-control processed as-received samples due to topography variations that led to the different orientations of normal vectors at each processed spot on the surface.

The rougher CoCrMo surfaces exhibited higher CA that was in line with the CB state analysis as they contained more air pockets compared to the polished disks.

The higher Saos-2 cells viability observed on the as-received disks was in agreement in previous studies; rougher surfaces offered better initial mechanical anchorage [21].

4.2 Effects of beam incident angle

When BIA deviations were introduced, the CA values increased with the BIA. This was attributed to the resulting increase of LIPSS periodicity as no other significant morphological differences were observed between samples processed with and without any BIA changes. Such a dependence was not reported by other researchers when investigated the BIA effects on polymer substrates, in particular after LIPSS processing of polystyrene or polyethyleneterephthalate samples [20, 29]. The wettability decrease of LST surfaces can be explained with the CB state. In particular, the higher periodicity led to relatively wider air pockets between the ripples and thus to the bigger air entrapment that led to a higher CA.

At the same time, a decrease in Saos-2 cell proliferation was observed on samples processed with higher BIA. This could be attributed again to the bigger ripples' periodicity. Knowing that cells anchor to the top of the sub-micron features [21, 30, 31], the longer periodicity implies that the seeded cells have to span larger distances in order to find anchoring points, thus this leads to less focal adhesion overall [31]. Other researchers observed the same interdependence between the cell proliferation and periodicity [20].

4.3 Effects of focal offset distance

When off-focus processing is performed or FOD is introduced in general, the effective spot size increases and hence laser fluence is reduced. Thus, any FOD variations shift the processing conditions away from the optimum fluence levels for LIPSS treatments of CoCrMo substrates and as a result the LIPSS depth gradually decreases until eventually no ripples are generated anymore. The diameter of a Gaussian beam at a distance z from the beam waist is given by [32]:

$$D(z) = D_0\sqrt{1+\left(\frac{z}{z_R}\right)^2} \quad (2)$$

where, D_0 is the beam diameter at the waist and z_R is the Rayleigh length. Thus for FOD of 0.2, 0.4, 0.6, and 0.8 mm, the respective beam diameters are 40.53, 42.09, 44.58, and 47.83 μm while the corresponding laser pulse fluence values are 195.3, 181.1, 161.4 and 140.3 mJ/cm^2. Thus, the relationship between the laser fluence and the depth of the sub-micron ripples appears to be linear on the polished CoCrMo disks within the investigated parameters' range (Table 2).

As a result of the FOD increase in this research, the corresponding fluence and LIPSS depth decreased and this had a detrimental effect on functional response of textured surfaces. In particular, the wettability of the CoCrMo surfaces decreased with the FOD increase. The FOD variations led to a CA increase initially (see Figure 7) when compared with the samples processed in-focus. Similar results were reported by Kietzig et al. when processing pure cobalt, i.e. the highest CA value was achieved at a fluence level lower than the highest one tested [33]. In addition, an off focus processing of copper and nickel surfaces to produce LIPSS was reported too, and again this led to higher CA values and a trend similar to that depicted in Figure 6 was discussed [34]. This suggests the existence of a specific sub-micron ripple depth, around 89 nm in this case, where the apparent CA is the highest. The CA values eventually decreased with the gradual loss of pattern due to the lower laser pulse fluence levels. The processing with a varying FOD had a detrimental effect on the proliferation of Saos-2 cells, too. Especially, the proliferation decreased and reached the lowest values at FOD of 0.4 mm and then slightly increased while remaining under the levels achieved without the focal offset. The FOD effects of the laser focal plane position were less pronounced than those of BIA on the proliferation of Saos-2 cells. Lamers et al. postulated the existence of a threshold LIPSS depth under which rat bone marrow cells were unable to respond to surface patterns on polystyrene [31]. This seems to be the case with samples processed with varying FOD; the gradual LIPSS depth decrease and ultimately the LST loss led to a gradual loss of the added surface functionalities, i.e. both surface wetting and Saos-2 proliferation.

4.4 Interdependences between wettability and Saos-2 cells proliferation

Looking at the impact of the two LST disturbances, the BIA and FOD deviations investigated in this research, on the wettability and Saos-2 cell proliferation data; it is clear that there is a correlation between them. In particular, a decrease of surface wettability, that is a CA increase, leads to a decrease of the Saos-2 cell proliferation. This is also confirmed by the Pearson correlation results reported in Table 3 where the average Pearson coefficient was close to –1. The correlation results did not show a strong agreement in the case of as-received/off-focus LST condition and this could be due to the high variations in height observed on the as-received samples, therefore the position of the focal plane relative to the surface is not always constant. To better visualize these trends, the surface functional responses were plotted against the different process disturbances in Figure 10. Therefore, any wettability changes can be used to explain and also to indicate for potential changes in the Saos-2 cell proliferation due to the effects on cells number/proliferation/metabolic activity on LST surfaces only and cannot be compared with non-structured surfaces (Figures 6–10). The mechanisms governing cell attachment and growth are different for structured surfaces. It is worth noting that any LST treatments with ultrashort lasers, such as a femtosecond laser source in this research, are carried out with a very low fluence (200 mJ/cm^2). In addition, the laser-material interaction time is extremely small (310 fs pulse duration) and therefore the temperature gradient

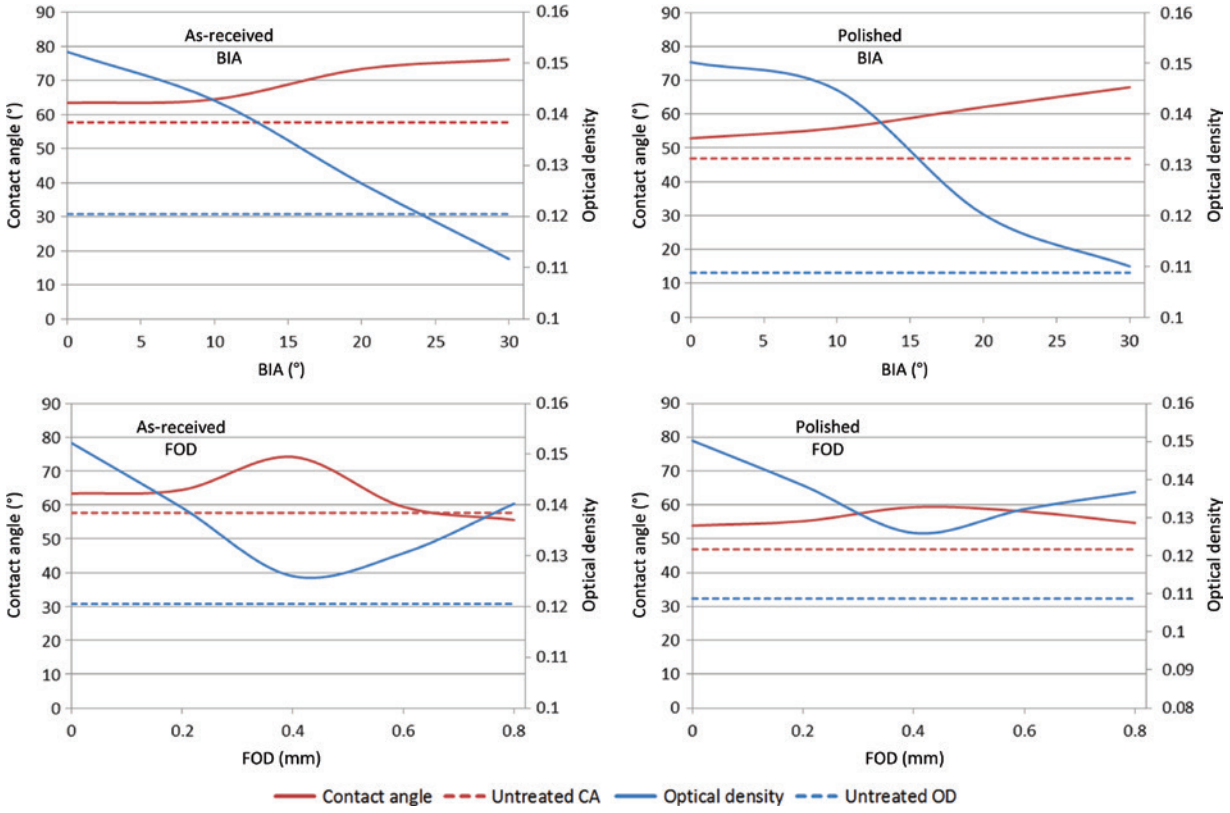

Figure 10: Interdependences between wettability and Saos-2 cells proliferation on laser treated CoCrMo disks.

can be considered negligible in the processed area. Thus, the surface chemistry is usually not affected and can be considered unchanged after laser processing. Therefore, any changes in wettability and cell proliferation can only be attributed to changes in the regular sub-micron topography. For example, the surface wettability could be used to explain the dip in Saos-2 cell proliferation at a beam defocusing distance of 0.4 mm and the subsequent increase at 0.8 mm. However, it should be stressed that the correlation between surface wettability and cell proliferation stands only when the LST surfaces are chemically and topographically comparable. This correlation could be used to judge the biological performance of LIPSS covered surfaces and determine the limits when transferring the added functionalities onto freeform implant surfaces and thus develop an adequate laser patching strategy.

5 Conclusion

The effects of LST disturbances on functional response of LIPSS treated CoCrMo disks with a NIR fs laser were investigated in this research. In particular, the FOD and BIA were varied to simulate the processing of a 3D part. The effects of these process disturbances on wettability and Saos-2 cell proliferation were analyzed. The following conclusions are derived based on the obtained results:

1. The LIPSS treatments enhanced the Saos-2 cells proliferation on the CoCrMo disks while their wettability decreased.
2. Irrespective of initial surface roughness there were substantial improvements in Saos-2 cells proliferation.
3. The biological response of laser-processed biomaterials is more sensitive to BIA changes compared with the effects of FOD variations, i.e. Saos-2 cells were more affected by changes in the periodicity of the sub-micron ripples rather than their depth.
4. The biological performance of biomaterials can be correlated to their wettability when the surfaces are chemically and topographically comparable.

Acknowledgments: The research was supported by two European Commission H2020 projects, the ITN programme 'European ESRs Network on Short Pulsed Laser Micro/Nanostructuring of Surfaces for Improved Functional Applications' (Laser4Fun) and the FoF programme 'High-Impact Injection Moulding Platform for mass-production of 3D and/or large micro-structured surfaces with

Antimicrobial, Self-cleaning, Anti-scratch, Anti-squeak and Aesthetic functionalities' (HIMALAIA). In addition, the work was carried out within the framework of the UKIERI DST programme 'Surface functionalisation for food, packaging, and healthcare applications'.

Author Contributions

A. Batal
Main author, conducted the laser experiments and functional tests.
A. Michalek
Assisted with LIPSS optimization and characterization.
A. Garcia-Giron
Assisted with sample preparation and wettability analysis.
V. Nasrollahi
Assisted with SEM imaging.
P. Penchev
Assisted with laser machining setup and supervision.
R. Sammons
Supervision and proofreading.
S. Dimov
Supervision and proofreading.

References

[1] T. Y. Liu and C. J. Kim, Science 346, 1096–1100 (2014).
[2] Q. L. Ma, L.-Z. Zhao, R.-R. Liu, B.-Q. Jin, W. Song, et al., Biomaterials 35, 9853–9867 (2014).
[3] T. Jwad, S. Deng, H. Butt and S. Dimov, Appl. Surf. Sci. 387, 617–624 (2016).
[4] L. Cheng, M. Liu, A. Mehta, H. Xin, F. Lin, et al., ACS Appl. Mater. Int. 7, 72073–72081 (2015).
[5] A. Garcia-Giron, J. M. Romano, Y. Liang, B. Dashtbozorg, H. Dong, et al., Appl. Surf. Sci. 439, 516–524 (2018).
[6] M. Gholami, M. Hoseinpoor and M. H. Moayed, Corr. Sci. 94, 156–164 (2015).
[7] Z. Y. Shi, Z. Q. Liu, H. Song and X. Z. Zhang, Appl. Surf. Sci. 364, 597–603 (2016).
[8] C. S. Kumar and S. K. Patel, Ceram. Intern. 44, 2510–2523 (2018).
[9] F. D. Arisoy, K. W. Kolewe, B. Homyak, I. S. Kurtz, J. D. Schiffman, et al., ACS Appl. Mater. Int. 10, 20055–20063 (2018).
[10] S. M. Bang, H.-J. Moon, Y.-D. Kwon, J.-Y. Yoo, A. Pae, et al., Clin. Oral Impl. Res. 25, 831–837 (2014).
[11] D. Bhaduri, P. Penchev, S. Dimov and S. L. Soo, Measurement 88, 248–261 (2016).
[12] I. Etsion, J. Tribol. 127, 248–253 (2005).
[13] X. W. Qi, H. Wang, Y. Dong, B. L. Fan, W. L. Zhang, et al., Tribol. Int. 135, 104–111 (2019).
[14] J. Dufils, F. Faverjon, C. Héau, C. Donnet, S. Benayoun, et al., Surf. Coat Tech. 329, 29–41 (2017).
[15] J. Bonse, S. Kirner, M. Griepentrog, D. Spaltmann and J. Krüger, Materials 11, 801 (2018).
[16] F. A. Shah, M. L. Johansson, O. Omar, H. Simonsson, A. Palmquist, et al., PLoS One 11 e0157504, (2016).
[17] D. C. Briski, B. W. Cook, J. M. Zavatsky and T. Ganey, Spine J. 15, S187 (2015).
[18] J. E. Sipe, J. F. Young, J. S. Preston and H. M. van Driel, Phys. Rev. B 27, 1141–1154 (1983).
[19] A. Cunha, O. F. Zouani, L. Plawinski, A. M. Botelho do Rego, A. Almeida, et al., Nanomed 10, 725–739 (2015).
[20] E. Rebollar, I. Frischauf, M. Olbrich, T. Peterbauer, S. Hering, et al., Biomaterials 29, 1796–1806 (2008).
[21] A. Batal, R. Sammons and S. Dimov, Mat. Sci. Eng. C 98, 1005–1013 (2019).
[22] I. Gnilitskyi, T. J.-Y. Derrien, Y. Levy, N. M. Bulgakova, T. Mocek, et al., Sci. Rep. 7, 8485 (2017).
[23] T. Mosmann, J. Immunol. Methods 65, 55–63 (1983).
[24] A. M. Prokhorov, A. S. Svakhin, V. A. Sychugov, A. V. Sychugov and A. A. Khakimov, Kvantovaya Elektronika 10, 906–912 (1983).
[25] A. Giacomello, S. Meloni, M. Chinappi and C. M. Casciola, Langmuir 28, 10764–10772 (2012).
[26] P. Bizi-Bandoki, H. S. Grewal, P. Pendyala, H. Shin, I. J. Cho, et al., Appl. Surf. Sci. 257, 5213–5218 (2011).
[27] M. Csete, O. Marti and Z. Bor, App. Phys. Mater. Sci. Pro. 73, 521–526 (2001).
[28] J. Reif, O. Varlamova and F. Costache, App. Phys. Mater. Sci. Proc. 92, 1019–1024 (2008).
[29] R. Krajcar, Mater. Let. 117, 184–187 (2014).
[30] A. Matsugaki, G. Aramoto, T. Ninomiya, H. Sawada, S. Hata, et al., Biomaterials 37, 134–143 (2015).
[31] E. Lamers, R. van Horssen, J. te Riet, F. C. M. J. M. van Delft, R. Luttge, et al., Eur. Cells Mater. 20, 329–343 (2010).
[32] D. Meschede, 'Optics, Light, and Lasers: The Practical Approach to Modern Aspects of Photonics and Laser Physics' (John Wiley & Sons, Hoboken, NJ, USA, 2017) pp. 1–528.
[33] A. M. Kietzig, M. N. Mirvakili, S. Kamal, P. Englezos and S. G. Hatzikiriakos, J. Adh. Sci. Technol. 25, 2789–2809 (2011).
[34] Y. C. Zhang, G. S. Zou, L. Liu, Y. Zhao, Q. Liang, et al., App Sur Sci 389, 554–559 (2016).

Afif Batal
Department of Mechanical Engineering, University of Birmingham, Edgbaston, Birmingham B15 2TT, UK
bxa361@student.bham.ac.uk

PhD student of the laser processing group in the Department of Mechanical Engineering at the University of Birmingham, UK.

Aleksandra Michalek
Department of Mechanical Engineering, University of Birmingham, Edgbaston, Birmingham B15 2TT, UK

PhD student of the laser processing group in the Department of Mechanical Engineering at the University of Birmingham, UK.

Antonio Garcia-Giron
Department of Mechanical Engineering, University of Birmingham, Edgbaston, Birmingham B15 2TT, UK

PhD student of the laser processing group in the Department of Mechanical Engineering at the University of Birmingham, UK.

Vahid Nasrollahi
Department of Mechanical Engineering, University of Birmingham, Edgbaston, Birmingham B15 2TT, UK. https://orcid.org/0000-0002-5697-8062

PhD student of the laser processing group in the Department of Mechanical Engineering at the University of Birmingham, UK.

Pavel Penchev
Department of Mechanical Engineering, University of Birmingham, Edgbaston, Birmingham B15 2TT, UK

Research fellow part of the laser processing group in the Department of Mechanical Engineering at the University of Birmingham, UK.

Rachel Sammons
School of Dentistry, University of Birmingham, Edgbaston, Birmingham B5 7EG, UK

Rachel Sammons is the Programme Lead for the BMedSc (Biomedical Materials Science) programme at the University of Birmingham. She is also the First Year Tutor and Examinations Officer for this Programme. Rachel Sammons research interests focus on surface interactions between mammalian cells and bacteria and biomaterials – especially titanium and hydroxyapatite, for bone repair and the prevention of infection.

Stefan Dimov
Department of Mechanical Engineering, University of Birmingham, Edgbaston, Birmingham B15 2TT, UK

Stefan Dimov is a Professor of micro manufacturing at the University of Birmingham. His research interests encompass the broad area of advanced manufacturing with a special focus on micro and nano manufacturing, additive manufacturing and hybrid manufacturing technologies. He established the micro manufacturing and hybrid manufacturing labs which are now widely recognised for their internationally leading research. His academic output includes more than 250 technical papers and 13 books. He has supervised over 20 PhD theses to completion. He has won in excess of £30M in external research grants and contracts.